Magnetic, thermal and transport properties of phase-separated La$_{0.27}$Nd$_{0.4}$Ca$_{0.33}$MnO$_3$

J Z Wang, J R Sun[1]**, G J Liu, F X Hu, R J Chen, T Y Zhao and B G Shen**

Beijing National Laboratory for Condensed Matter Physics and Institute of Physics, Chinese Academy of Sciences, Beijing 100080, People's Republic of China

E-mail: jrsun@g203.iphy.ac.cn

Abstract

The magnetic, resistive and thermal properties of the phase-separated compound La$_{0.27}$Nd$_{0.4}$Ca$_{0.33}$MnO$_3$ have been experimentally studied. The sample is found to experience a charge/orbital ordering transition at ∼175 K and an antiferromagnetic (AFM) transition at ∼156 K without a magnetic field. A magnetic field stabilizes the ferromagnetic (FM) order and the field-induced FM phase coexists with the AFM phase under a field below 2 T in the temperature range below $T_C \approx 110$ K. However, the magnetic entropy change accompanying the AFM–FM transition is negligibly small when $T_C < T_N$, grows rapidly as T_C approaches T_N under the driving of an applied field, and saturates at a value of ∼4 J kg^{-1} K^{-1} when $T_C > T_N$. A general relation between resistivity and magnetization, $\rho = A_0 T \exp[(\varepsilon - 800m^2)/T]$ (m = normalized magnetization), is established for the paramagnetic phase, which is also applicable to other compounds with different characters, such as the La$_{0.67}$Ca$_{0.33}$MnO$_3$ film and the La$_{0.474}$Bi$_{0.193}$Ca$_{0.33}$Mn$_{0.994}$Cr$_{0.006}$O$_3$ and Eu$_{0.55}$Sr$_{0.45}$MnO$_3$ ceramics. In the FM state, the resistivity is quite sensitive to the change of spin alignment and exhibits an exponential decrease with magnetization $\rho = \rho_0 \exp(-22.7m)$. Field-induced phase separation is believed to be responsible for the distinct properties of La$_{0.27}$Nd$_{0.4}$Ca$_{0.33}$MnO$_3$.

(Some figures in this article are in colour only in the electronic version)

1. Introduction

Perovskite manganites have received a great deal of attention primarily due to their colossal magnetoresistance (CMR) properties [1]. Subsequent work revealed the presence of abundant physics associated with strongly coupled spin, charge and orbital degrees of freedom in the manganites [2, 3]. In addition to the familiar spin ordering, occurrences of charge and orbital ordering under appropriate conditions, which led to periodic arrangements of both the position and orientation of the d$_{3z^2-r^2}$ or d$_{x^2-y^2}$ orbitals, have been experimentally proved. Accompanying the charge and orbital ordering, the resistivity exhibits a sudden jump while the magnetization experiences a steep drop if the compound is originally in a

ferromagnetic (FM) state, or an obvious hump if the compound is in a paramagnetic (PM) state. Any external stimuli that affect the spin, charge and orbital orderings can result in dramatic effects [3–5].

In general, the tendency to the charge and orbital ordering can be enhanced by weakening the double exchange interaction, which can be realized by simply replacing La in the manganite with, for example, Pr or Nd [6–9]. One of the most distinctive features in the Pr/Nd-doped manganite is the occurrence of phase separation, that is, two or more phases coexist in a wide temperature range. The coexisting metallic and insulating domains are found to be sub-micrometer in size, and the latter are usually charge-ordered. Different from the typical manganite La$_{2/3}$(Sr/Ca)$_{1/3}$MnO$_3$ [10, 11], for which two phases coexist in a narrow temperature range around T_C and the proportion of each phase depends strongly

[1] Author to whom any correspondence should be addressed.

on both temperature and magnetic field, the phase separation in $La_{1-x-y}(Pr/Nd)_yCa_xMnO_3$ occurs in a wide temperature range below T_C, and usually varies with applied field but not temperature.

Phase separation can lead to a much more complex magnetic behavior. Taking $La_{5/8-x}Pr_xCa_{3/8}MnO_3$ ($x = 0.35$) as an example [6–8], it undergoes, with the decrease of temperature, first a phase transition at $\sim$200 K that yields a parasitical FM state, then an FM transition at $\sim$110 K. The first phase transition occurs accompanied by a charge/orbital ordering, which results in the significant suppression of the magnetic order. However, a field above 2 T can depress the charge and orbital ordering, driving the compound to a completely FM state. As a consequence, a huge magnetoresistance appears. This effect is especially strong in bar-shaped samples with a width of micrometers, and a magnetoresistance of 10 000-fold can result [12]. Because of the comparability of the sample dimension and the domain sizes of coexisting phases, the magnetic field affects resistivity mainly by melting the insulating domains that block the conduction paths. In addition to the magnetic field, an electric field can also influence the resistivity [12–14], and a collapse of conduction percolation due to the effects of local heating by strong current was also observed [15].

One of the most important characteristics of the manganites is the strong magnetic and resistive interplay. In general, resistivity will decrease as magnetization (M) increases, regardless of the magnetic state. This has stimulated an exploration for a general relation between ρ and M. For the typical CMR manganite $La_{0.7}Ca_{0.3}MnO_3$, Hundley *et al* [16] established a simple relation of $\rho = \rho_0 \exp(-\beta m)$, where $m = M/M_S$ is the normalized magnetization (M_S = saturation magnetization) and β is a constant. This relation means that all of the (ρ, m) pairs collected under different temperatures and magnetic fields collapse into the same master curve, and has been regarded as evidence of polaron decomposition during the PM–FM transition. In the temperature range above T_C, Urushibara and colleagues [17] found $\rho = \rho_0(1 - Cm^2)$ for $La_{1-x}Sr_xMnO_3$, where C is a constant depending on Sr content. Different from this, Chen *et al* [18] established a relation of $\rho = \rho_0 \exp(-\alpha m^2/T)$ for $La_{0.67}Ca_{0.33}MnO_3$ (the Boltzmann constant k_B has been set to unity). These studies were performed for the manganites without significant phase separation. Kim *et al* [7] analyzed the ρ–T relation of $La_{5/8-x}Pr_xCa_{3/8}MnO_3$ using the effective medium model, and successfully reproduced the observed transport behavior in the temperature range around the metal-to-insulator (M–I) transition.

We noticed that most of the previous work concentrated mainly on Pr-doped $La_{1-x}Ca_xMnO_3$ [6–8], for which the charge/orbital ordering and the antiferromagnetic (AFM) ordering occur nearly simultaneously and coexist with a weak FM ordering. This makes it difficult to get a close view of the evolution of the spin, charge and orbital orderings against magnetic field and temperature. $La_{0.27}Nd_{0.4}Ca_{0.33}MnO_3$ (LNCMO) is a compound that exhibits compatible AFM and FM interactions. With the decrease of temperature, it undergoes first a charge/orbital ordering then an AFM

transition, both of which can be readily detected by magnetic, thermal and resistive measurements. A magnetic field of a few teslas can overturn the stability of the AFM order, resulting in the coexistence of AFM and FM phases. Similar features to those of LNCMO were also observed in other manganites doped by small rare-earths, such as $Eu_{1-x}Sr_xMnO_3$, $Sm_{1-x}Sr_xMnO_3$ and $Pa_{1-x}(Ca, Sr)_xMnO_3$, etc [12, 19–22]. This means that LNCMO and related compounds compose a large family for which the FM order emerges and develops in the AFM matrix under an applied field. This feature of the compounds allows a quantitative investigation of the effects associated with phase separation, which could be helpful for revealing hidden aspects of phase-separated manganites.

In this paper, the magnetic, thermal and resistive properties of LNCMO are systematically studied. Special attention has been paid to the effects associated with phase separation, particularly the evolution of each phase with magnetic field and temperature, which leads to the establishment of a magnetic phase diagram in the temperature–magnetic field plane. We have tried to give quantitative descriptions of the magnetic–resistive correlation for the PM phase, the mixed FM and PM and/or AFM phases, and the FM phase, respectively, and the magnetic entropy changes associated with the magnetic field-induced AFM–FM transition. The generality of the results obtained for LNCMO are also checked by a comparison study of other manganites with similar or different features to LNCMO, a $La_{0.67}Ca_{0.33}MnO_3$ film on an $SrTiO_3$ substrate and two ceramics $La_{0.474}Bi_{0.193}Ca_{0.33}Mn_{0.994}Cr_{0.006}O_3$ and $Eu_{0.55}Sr_{0.45}MnO_3$.

2. Experiments

A polycrystalline sample LNCMO was prepared by the conventional solid-state reaction method. Well-mixed stoichiometric amounts of the La_2O_3, Nd_2O_3, $CaCO_3$ and $MnCO_3$ powders were calcined first at 1000 °C for 24 h then at 1250 °C for 48 h, with an intermediate grinding for homogenization. The resultant product was ground, pelletized and sintered at 1350 °C for another 36 h, then furnace-cooled to room temperature. For a comparison study, another two polycrystalline samples $La_{0.474}Bi_{0.193}Ca_{0.33}Mn_{0.994}Cr_{0.006}O_3$, $Eu_{0.55}Sr_{0.45}MnO_3$ and a $La_{0.67}Ca_{0.33}MnO_3$ epitaxial film grown on a $SrTiO_3$ substrate ($\sim$200 nm in thickness) were also prepared following the procedures described in [23, 20] and [24], respectively.

The phase purity and crystal structure of the LNCMO sample were studied by powder x-ray diffraction performed by a Rigaku x-ray diffractometer with a rotating anode and Cu Kα radiation. The magnetic and resistive data were recorded by a Quantum Design superconducting quantum interference device magnetometer (MPMS-7) equipped with an electric measurement unit. A physical property measurement system (PPMS-14H) was used for the measurements of heat capacity.

To eliminate spurious effects, exactly the same sample was used for all the measurements. The LNCMO specimen was first shaped to $8 \times 1.5 \times 1$ mm^3 for resistivity measurements.
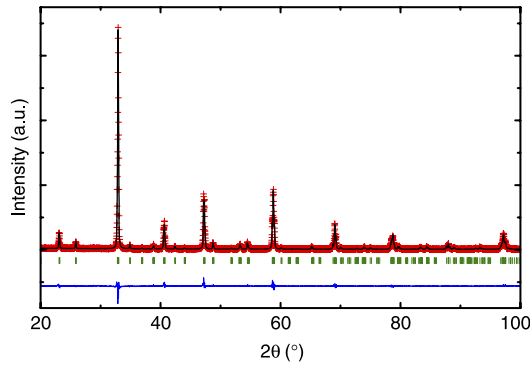
Figure 1. Observed (crosses) and calculated (continuous line) x-ray diffraction patterns of LNCMO. The difference between the experimental and theoretical data is plotted at the bottom of the figure. Vertical bars denote the calculated positions of the Bragg reflections ($R_{wp} = 17.5\%$, $R_e = 14.6\%$).

After that, the middle part of the bar-shaped sample was cut into small pieces for subsequent magnetic and thermal measurements. Unless specially specified, all the data presented here were collected in the warming process after cooling the sample to predetermined temperatures without a magnetic field.

3. Results and discussion

3.1. Crystal structure

As revealed by the Rietveld analysis of the powder x-ray diffraction spectrum collected at room temperature (figure 1), the LNCMO sample is a single phase of orthorhombic structure (space group *Pbnm*) with the lattice parameters of $a = 0.5434$ nm, $b = 0.5456$ nm and $c = 0.7671$ nm. The relation $b > a > c/\sqrt{2}$ is a signature of an O′-type structure. The unit-cell volume is 0.227 nm³, ∼0.8% smaller than that of $La_{0.67}Ca_{0.33}MnO_3$ [9]. This is possibly the consequence of the partial replacement of Nd for La, and is expected to have a strong impact on the magnetic and resistive properties of LNCMO.

$La_{0.474}Bi_{0.193}Ca_{0.33}Mn_{0.994}Cr_{0.006}O_3$, $Eu_{0.55}Sr_{0.45}MnO_3$ and $La_{0.67}Ca_{0.33}MnO_3$ film are also single-phase samples. The $La_{0.67}Ca_{0.33}MnO_3$ film is found to be highly textured, with the quality of a single crystal. The corresponding structural parameters have been reported in [23, 20] and [25].

3.2. Magnetic phase diagram

Figure 2(a) shows the temperature-dependent magnetization of LNCMO measured under various magnetic fields between 0.02 and 5 T. Two obvious magnetic anomalies, occurring at $T_C \approx$ 90 K and $T_{CO} \approx 175$ K, respectively, can be identified from the M–T curve obtained under the field of 0.02 T. The former is a signature for the appearance of a weak FM phase which can be a result of the strong (s–d)/(d–d) exchange such as that observed in $(Eu/Sm)_{0.55}Sr_{0.45}MnO_3$, etc [26, 27], while the latter is a typical feature of a charge ordering (CO) transition.
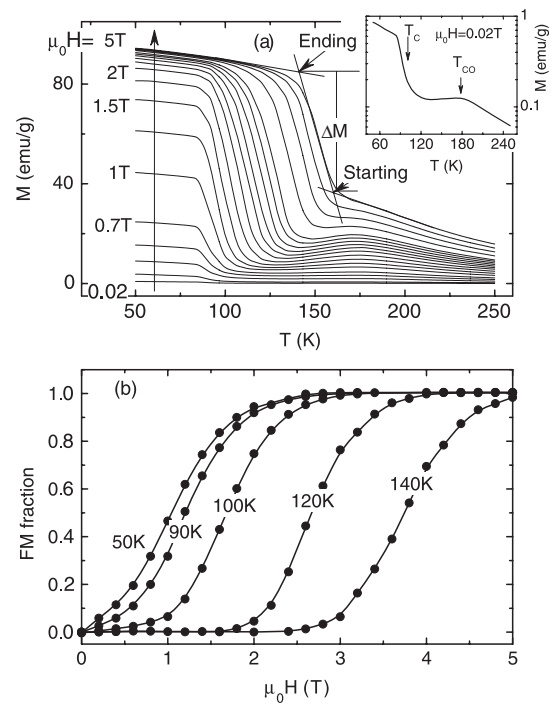

Figure 2. (a) Temperature-dependent magnetization measured under fields between 0.02 and 5 T. The step size of magnetic field selected is ∼0.2 T between 0.02 and 2 T, and 0.5 T between 2 and 5 T. The straight lines demonstrate the definition of the starting and ending temperatures for the phase transition. (b) Volume fraction of FM phase (X_{FM}) as a function of magnetic field at the temperatures of 50, 90, 100, 120 and 140 K. X_{FM} is defined as $X_{FM} = (M - M_{AFM})/(M_{FM} - M_{AFM})$, where M_{FM} and M_{AFM} are the magnetization in the complete FM and AFM state, respectively. Also see [20].

The magnetic behaviors of LNCMO exhibit a magnetic field-dependent feature. The Curie temperature T_C, defined as the temperature corresponding to the minimum of dM/dT, varies significantly with external field, growing from ∼90 to ∼180 K as the field increases from 0 to ∼9 T (refer to the heat capacity data presented in section 3.3). Accompanying the increase of T_C, the FM state is considerably stabilized. Its volume fraction, in the temperature range below 90 K, increases from ∼10% to ∼90% as the magnetic field sweeps from ∼0.5 to ∼2 T, according to the analysis of isothermal magnetization data. This actually implies the coexistence of two phases in a wide temperature range below T_C (figure 2(b)). All the magnetic phases below ∼90 K are converted into the FM one by a magnetic field above 2 T. The slight increase of magnetization for $\mu_0 H > 2$ T arises from the spin aligning in FM domains. The saturation magnetization is ∼3.63 μ_B/Mn, obtained by extrapolating the M–T curve under 5 T to 0 K. This result is in good agreement with the expected value 3.67 μ_B/Mn if only the magnetic moment of Mn ions is considered.

Compared to the compound with a similar Ca content $Nd_{0.625}Ca_{0.375}MnO_3$ [28], the critical temperature for the CO transition of LNCMO is considerably lower (∼225 K versus ∼175 K). The magnetic field is found to weakly affect the CO transition, causing a slight decrease of T_{CO} at the rate of ∼1.54 K T⁻¹, which can be a consequence of field-induced delocalization of the e_g electrons. However, the CO state
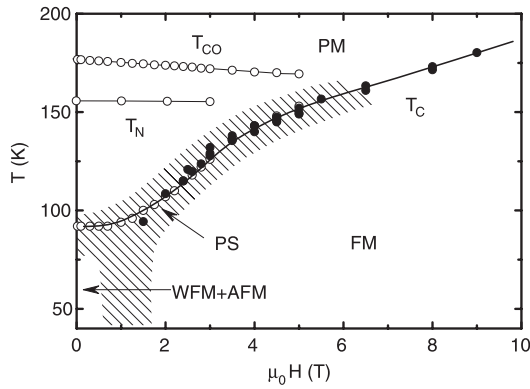
Figure 3. Phase diagram of LNCMO depicted in the magnetic field–temperature plane. Open and full circles represent magnetic and thermal data, respectively. The hatched area marks the region where two phases coexist. WFM = weak ferromagnetic phase; PS = phase separation.

Figure 4. Heat capacity of LNCMO as a function of temperature measured without an external field. The obvious upturn below ~15 K, marked by an arrow, is due to a thermal excitation of Nd^{3+} ions in a crystalline field. The inset plot is a close view of the effects of phase transitions. The critical temperatures of the AFM and charge ordering transitions are marked by arrows.

remains stable up to the field of 5 T, as shown by the visible magnetic anomaly around 175 K in the M–T curve (figure 2(a)).

Figure 3 is a phase diagram of LNCMO depicted on the T–$\mu_0 H$ plane. T_C is nearly constant when the magnetic field is low, and increases first rapidly then slowly as the field sweeps from ~1.5 to ~9 T, yielding an 'S'-shaped T_C–$\mu_0 H$ relation. This behavior is different from that usually observed in other manganites. The heat capacity data reveal the occurrence of an AFM transition at $T_N \approx 156$ K, independent of the applied field. It is interesting to note that the T_C–$\mu_0 H$ curve is curved for $T_C < T_N$ and nearly linear otherwise. This result suggests a close relation between the complex T_C–$\mu_0 H$ dependence and the AFM–FM transition. The T_C–$\mu_0 H$ slope is ~14.0 K T^{-1} for 100 K < T_C < T_N and ~7.6 K T^{-1} for $T_C > T_N$. This means that it is easier for the magnetic field to push the Curie temperature upwards in the AFM background than in the PM one.

The hatched area in figure 3, the edges of which are determined by the starting/ending temperatures of the phase transition shown in figure 2(a), marks the region of phase separation. It shows that the FM and AFM (or PM) phases coexist below (above) ~156 K. Although phase separation was also observed in $La_{0.67}(Ca/Sr)_{0.33}MnO_3$ in the vicinity of T_C [10, 11], for which the double exchange coupling is believed to be dominant, the two phases coexistence in a wide temperature range below T_C, like that in the present sample, only occurs when La is properly replaced by smaller rare-earth atoms such as Nd, Pr, etc, and is expected to affect the thermal and electronic transport properties of the compound.

3.3. Thermal effects of phase transition

To get knowledge about the thermal effects of the phase transition, which contains valuable information on the relation between different magnetic phases, the thermal property of LNCMO is further studied. As shown in figure 4, the heat capacity (C_p) of LNCMO exhibits a smooth growth with the increase of temperature until the appearance of an obvious concavity near $T_N \approx 156$ K, which is a signature of the AFM
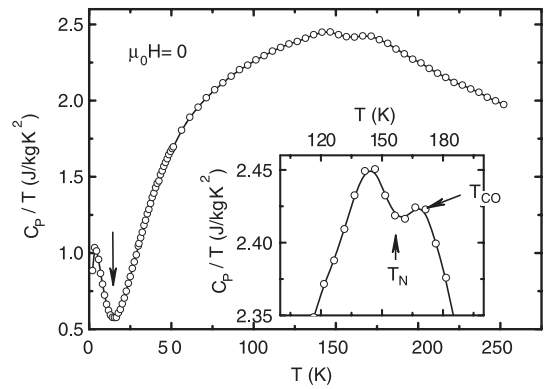
transition. As will be seen below, the AFM order in LNCMO is robust, persisting up to the field of ~3 T, with an essentially unaffected critical temperature. A similar AFM transition was also observed in $Nd_{0.5}Ca_{0.5}MnO_3$, though the magnetic anomaly in the M–T curve was rather weak. It appears even when the Ca content deviates significantly from 0.5 [28, 29]. Furthermore, the CO transition can also be identified from the thermal data, and it is signified by a visible hump in the C_p/T–T curve. The obvious upturn below ~15 K is due to an excitation of the magnetic state of the Nd^{3+} ions in the crystalline field [30]. According to the magnetic and thermal data, there are in total three phase transitions in sequence as temperature increases, which lead the system from the weak FM state first to the AFM state, then the PM state. Meanwhile, the AFM and PM states are also charge-ordered when $T < T_{CO}$.

Figure 5 shows the heat capacity of LNCMO measured under selected fields between 0 and 8 T in the temperature range around the phase transitions (100–200 K). Unexpectedly, there is no thermal response to the FM transition when the magnetic field is lower than 2.5 T, though both the magnetic and resistive data (refer to the following section 3.4 for resistive data) confirm the occurrence of this transition. A thermal anomaly, shown as a C_p peak around T_C, emerges and develops as the field sweeps from 3 to 8 T (inset plot in figure 5). The peak position is located at T_C, and the peak height quantifies the thermal exchange accompanying the phase transition. Figure 6 exemplifies the corresponding magnetic entropy change calculated by

$$\Delta S = \int_{T_1}^{T_2} \frac{\Delta C_p \mathrm{d}T}{T},\tag{1}$$

where ΔC_p is the magnetic contribution obtained by subtracting the smooth background, determined by a polynomial fitting, from the total heat capacity and $\Delta T = T_2 - T_1$ is the temperature span of the magnetic transition. Different symbols in the figure mark the data recorded in different cycles of the experiments. It is obvious that the
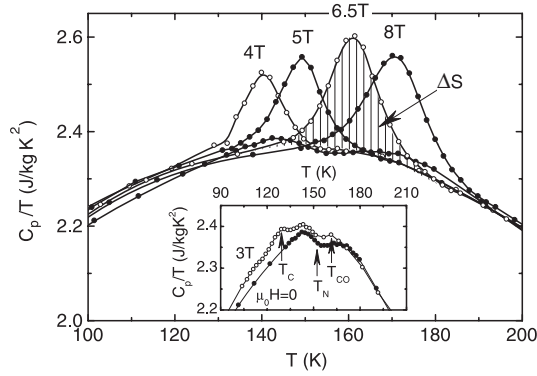
Figure 5. Heat capacity of LNCMO measured under different magnetic fields in the temperature range around phase transitions. The inset plot is a close view of the heat capacity under the fields of 0 and 3 T. An obvious thermal anomaly around T_C can be observed when the magnetic field exceeds 3 T. The hatched area marks the entropy change as a result of the FM transition. Solid lines are guides for the eyes.
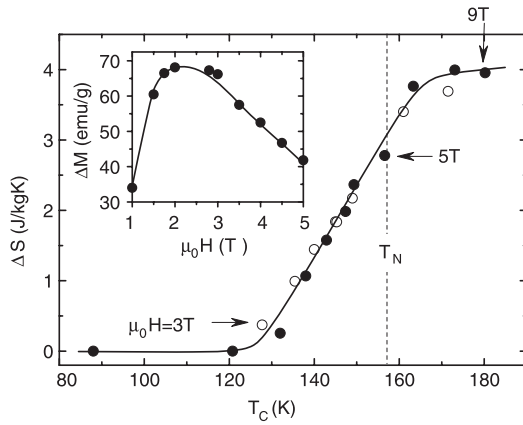

Figure 6. Magnetic entropy change resulting from the FM transition as a function of Curie temperature. Open and full circles represent two sets of experiment data obtained by repeating the heat capacity measurements. The inset plot shows the variation of magnetization accompanying the FM transition.

thermal effects begin to appear when T_C exceeds $\sim$130 K, grows drastically as T_C sweeps through $\sim$130–160 K and nearly saturates above $\sim$160 K. The maximal ΔS, obtained under the field of 9 T, is $\sim$4 J kg^{-1} K^{-1} or $\sim$0.19 k_B/Mn, in good agreement with the values of La$_{0.7}$Ca$_{0.3}$MnO$_3$ and La$_{0.7}$Sr$_{0.3}$MnO$_3$ ($\sim$0.2 k_B/Mn) [31]. This result indicates that LNCMO behaves like an ordinary manganite above $\sim$160 K.

In general, the thermal anomaly is expected to enhance with ΔM, the magnetization drop at T_C. As shown in the inset plot in figure 6, ΔM exhibits first a steep increase with magnetic field, which leads to a broad maximum of $\sim$63 emu g^{-1} around $\mu_0 H \approx 2.5$ T, then a rapid decrease for $\mu_0 H > 3$ T. The first process is associated with the field-induced growth of FM domains, while the second one is due to the magnetization increase of the PM phase under high applied fields. According to figure 6, however, ΔS appears and develops only above the field of 3 T. This result indicates the absence of a direct correlation between ΔS and ΔM.
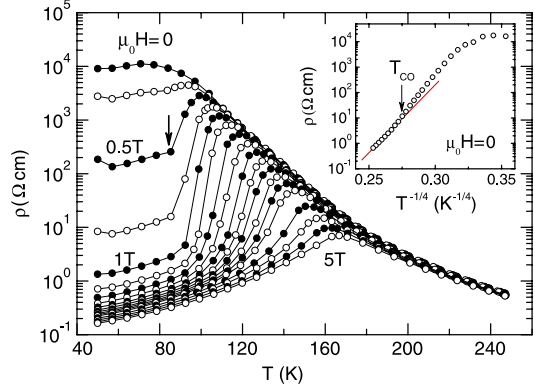

Figure 7. Temperature-dependent resistivity of LNCMO measured under various magnetic fields. The arrow marks the corner in the resistivity curve, resulting from phase separation. The inset plot shows the resistive anomaly associated with the CO transition.

As shown in figure 3, the Curie temperature increases monotonically with applied field, and it will sweep through T_N because the latter remains essentially constant. Thermal effects appear only when T_C and T_N are close enough and saturate soon for $T_C > T_N$ (figure 6). According to the heat capacity data, LNCMO experiences an AFM transition that proceeds in a broad temperature region. The visible hump around $\sim$150 K in the C_p/T–T curve is obviously a consequence of the expansion of the lambda-shaped transition (figures 4 and 5). The broad magnetic transition indicates the inhomogeneity of the compound, probably due to grain boundaries and/or structural defects [32]. In the case of $T_C < T_N$, the compound undergoes first a PM–AFM then an AFM–FM transition on cooling, while only a PM–FM transition when $T_C > T_N$. Considering the absence of ΔS when T_C is much lower than T_N, the thermal effects of the AFM–FM transition could be negligibly weak, and the thermal anomaly arises mainly from the PM–FM transition. This explains the observation that the drastic ΔS increase takes place only in a narrow temperature range around T_N. In this temperature region, the AFM and PM phases coexist and the proportion of the PM phase, and thus the contribution of the PM–FM transition, grows as the temperature approaches T_N. Only the PM phase survives above T_N and, as a result, the rapid increase of ΔS slows down.

3.4. Magnetic and resistive interplay

In addition to the distinctive thermal effects associated with the magnetic transition, the resistive behavior of LNCMO displays a complex variation with the change in magnetic state. As shown in figure 7, the sample exhibits an insulating behavior without the magnetic field, with a visible anomaly at $\sim$175 K due to the CO transition (inset in figure 7). Accompanying the emergence of the field-induced FM ordering, an incomplete, however visible, resistive transition appears at $T_P \approx 99$ K under the field of 0.5 T. As the population of the FM phase grows further under higher applied fields, the transition becomes more evident and a resistivity drop of three orders of magnitude appears, in addition to the high temperature shift of T_P. Two distinctive features can be identified from the $\rho(T)$
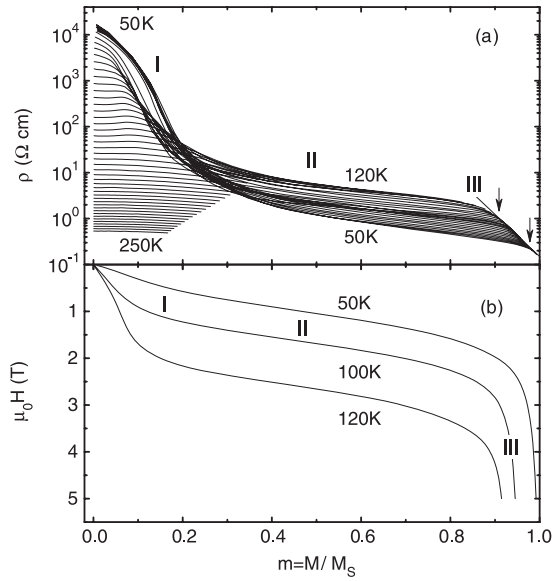
Figure 8. (a) Isothermal resistivity–magnetization curves obtained at different temperatures between 50 and 250 K with a step size of 5 K. (b) Magnetization as a function of magnetic field. Only three curves for $T = 50$, 100 and 120 K are shown for clarity. Numbers in the figures mark different electronic and magnetic processes. The two arrows and the straight line mark the resistivity change of the FM phase with m.

curves of LNCMO. The first one is the presence of a rigid corner near ∼85 K (marked by an arrow) due to the slowdown of the resistivity drop below T_P, and the second one is the parallelism of the ρ–T curves in the low temperature range (50–80 K) measured under the fields between 0.5 and 5 T. These behaviors were also observed in La$_{5/8-x}$Pr$_x$Ca$_{3/8}$MnO$_3$, another typical phase-separated manganite [7].

In general, for the manganite the resistivity decreases as magnetization grows, regardless of the magnetic state. Urushibara *et al* [17] found that $\rho(m) = \rho_0(1 - Cm^2)$ for the PM phase of La$_{1-x}$Sr$_x$MnO$_3$, where $m = M/M_S$ is the normalized magnetization and C is a constant varying between ∼1.2 and ∼4, depending on Sr content. In contrast, Chen *et al* [18] proposed a relation of $\rho(m, T) = \rho_0 \exp(-\alpha m^2/T)$ for La$_{0.67}$Ca$_{0.33}$MnO$_3$ with $\alpha \approx 1600$ K. For the FM state, there is also a definite relation between ρ and m $\rho(m, T) = \rho_0 \exp(-\beta m)$, given by Hundley *et al* for La$_{0.7}$Ca$_{0.3}$MnO$_3$ [16], where β is a constant independent of temperature and magnetic field.

It should be noted that these results have been obtained for the manganites in which phase separation, if it occurs, exists only in a very narrow temperature range around T_C. These compounds are in a good FM state in the temperature range well below T_C, with the magnetic structures insensitive to external stimuli. LNCMO is different in the sense that its phase separation is induced by an external field and persists in a wide temperature range below T_C. Therefore, what the ρ–M relation is in LNCMO is an issue requiring further study.

Combining the data in figures 2 and 7, we obtain the isothermal ρ–m relations shown in figure 8(a). In the temperature range well below T_C, three processes can be

identified: (I) the rapid decrease of resistivity as magnetization sweeps through $m \approx 0.15$, (II) the following smooth reduction above $m \approx 0.25$ and (III) the downward curvature of the ρ–m curves as m approaches saturation. In sharp contrast to the results of La$_{0.7}$Ca$_{0.3}$MnO$_3$ obtained by Hundley *et al* [16], the resistivity of LNCMO is different at different temperatures even if magnetization is fixed. With the increase of temperature, the first process becomes ambiguous, due to the smoothening of the drastic change of ρ with m. The first two processes merge into a unified one above T_C, and the isothermal ρ–m curves at different temperatures are nearly parallel with each other, downwards shifting as the temperature increases. Changes of magnetization against applied field are shown in figure 8(b). It is obvious that the first two processes correspond to the rapid growth of the FM phase, while the last one corresponds to the improvement of the spin alignment in the FM domains after all the magnetic phases are converted into the FM one.

It is evident that the ρ–m relation is different for different magnetic states. Let us consider the ρ–m relation of the PM phase first. Figure 9(a) presents ρ as a function of m^2/T for LNCMO. It shows excellently linear ln ρ–m^2/T curves with a nearly constant negative slope of ∼800 K. This actually indicates a relation of $\rho(m, T) = \rho_0(T) \exp(-\alpha m^2/T)$, the same result as that obtained by Chen *et al* [18] except for a smaller coefficient α (∼800 K versus ∼1600 K). It means that the variation of magnetization will considerably affect resistivity even in the PM state. The effect thus produced could be strong especially at low temperatures, and a simple calculation shows that, for example, MR = $[\rho(0, T) - \rho(m = 0.3, T)]/\rho(0, T)$ is ∼0.37 at 160 K and ∼0.26 at 250 K.

This relation also exists in other manganites of different characteristics. Figure 9(b) illustrates the ρ–m^2/T dependence of the La$_{0.67}$Ca$_{0.33}$MnO$_3$ film on a SrTiO$_3$ substrate and the ceramics La$_{0.474}$Bi$_{0.193}$Ca$_{0.33}$Mn$_{0.994}$Cr$_{0.006}$O$_3$ and Eu$_{0.55}$Sr$_{0.45}$MnO$_3$. Not only an exponential dependence between ρ and m but also, fascinatingly, essentially the same ln ρ–m^2/T slopes as those of LNCMO are observed (inset plot in figure 9(b)). As we know, the La$_{0.67}$Ca$_{0.33}$MnO$_3$ film is a typical manganite with an idealized M–I transition. In contrast, La$_{0.474}$Bi$_{0.193}$Ca$_{0.33}$Mn$_{0.994}$Cr$_{0.006}$O$_3$ and Eu$_{0.55}$Sr$_{0.45}$MnO$_3$ exhibit a field-dependent phase separation and the M–I transition takes place only under a high applied field as a consequence of the percolation of the FM phase. In addition to this, significant short-range magnetic order exists in Eu$_{0.55}$Sr$_{0.45}$MnO$_3$ above T_C [20].

Figure 10 presents the experimental data of the La$_{0.67}$Ca$_{0.33}$MnO$_3$ film plotted in a semi-logarithmic or a linear scale. A satisfactory description is given only by the former when m is large. All these reveal the universality of the ρ–m relation obtained. It captures the essence of the magnetic–resistive interplay in manganites. As a supplement, we would like to point out that the $\rho(m) = \rho_0(1 - Cm^2)$ relation, proposed by Urushibara *et al* [17], is a natural inference of the formula $\rho(m, T) = \rho_0(T) \exp(-\alpha m^2/T)$ when m is small, with $\alpha = CT$. Using the parameters of $C \approx 2.15$ and $T = 1.01T_C \approx 373$ K in [17], we obtain $\alpha \approx 802$ K for this La$_{0.7}$Sr$_{0.3}$MnO$_3$ single crystal. This is a result similar to those of other samples studied here.
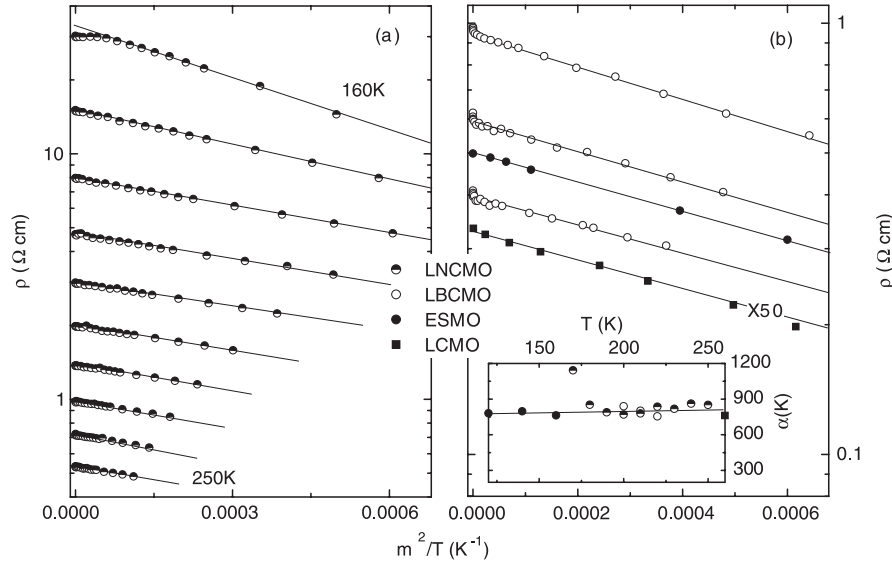
Figure 9. Semi-log plot of resistivity as a function of m^2/T obtained at different temperatures for (a) LNCMO and (b) La$_{0.67}$Ca$_{0.33}$MnO$_3$ film, La$_{0.474}$Bi$_{0.193}$Ca$_{0.33}$Mn$_{0.994}$Cr$_{0.006}$O$_3$ and Eu$_{0.55}$Sr$_{0.45}$MnO$_3$ ceramics. The inset plot shows the $\ln\rho$–m^2/T slope for different manganites at various temperatures. LBCMO = La$_{0.474}$Bi$_{0.193}$Ca$_{0.33}$Mn$_{0.994}$Cr$_{0.006}$O$_3$, ESMO = Eu$_{0.55}$Sr$_{0.45}$MnO$_3$ and LCMO = La$_{0.67}$Ca$_{0.33}$MnO$_3$ film.

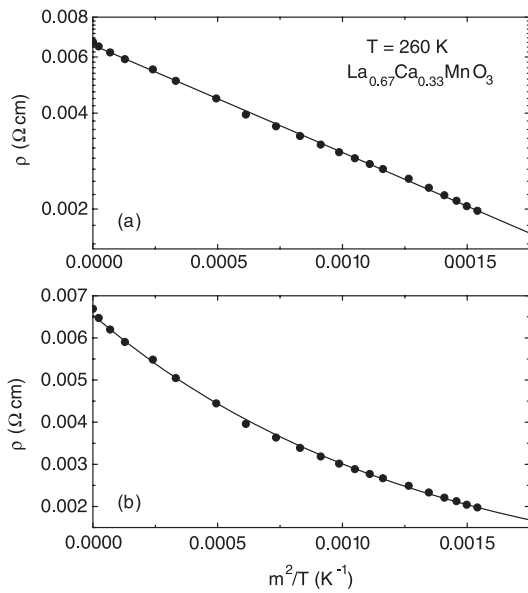**Figure 10.** A comparison of the (a) $\ln\rho$–m^2/T and (b) ρ–m^2/T relations for the La$_{0.67}$Ca$_{0.33}$MnO$_3$ film obtained at the temperature of 260 K. Solid lines are guides for the eyes.

The downward shift of the $\ln\rho$–m^2/T curve with the increase of temperature originates from $\rho_0(T)$, for which usually a picture of adiabatic polaronic transport $\rho(T) = A_0 T \exp(\varepsilon/T)$ is adopted, where ε is the energy required to excite polarons. Therefore, the general expression for the transport behavior of the PM phase will be

$$\rho = A_0 T \exp\left(\frac{\varepsilon - \alpha m^2}{T}\right). \quad (2)$$

For the FM phase below T_C, however, the simple relation of $\rho(m, T) = \rho_0 \exp(-\beta m)$ proposed by Hundley *et al* [16]

does not hold for LNCMO. The resistivity exhibits a very complex variation with the increase of m, strongly depending on temperature. It could be a consequence of phase separation: ρ is expected to vary when the volume fractions of the AFM and FM phases change even if m is constant. In general, the resistivity of a system with two randomly distributed phases can be described by the effective medium theory [7]:

$$(1-f)\left(\frac{\sigma_I^{1/t} - \sigma^{1/t}}{\sigma_I^{1/t} + A\sigma^{1/t}}\right) + f\left(\frac{\sigma_m^{1/t} - \sigma^{1/t}}{\sigma_m^{1/t} + A\sigma^{1/t}}\right) = 0, \quad (3)$$

where $A = (1 - f_c)/f_c$, f_c is the threshold volume fraction for a three-dimensional percolation. σ_I is the conductivity of the insulating phase (AFM phase) and it is approximated by the conductivity without an external field. σ_m is the conductivity of the metallic phase (FM phase). Figure 11 is a comparison of the observed and calculated ρ–m relations at selected temperatures. A satisfactory description of experimental results is obtained in a wide m range by properly choosing the parameters t and f_c. The percolation threshold f_c adopted by the calculation varies between 0.11 and 0.14, close to the theoretical value of 15%. According to this analysis, the drastic variation of ρ near $m = 0.15$ is a result of the FM percolation, while the smooth decrease above $m \approx 0.25$ could be ascribed to the continuous growth of FM domains above percolation.

The parameter t exhibits a systematic variation with temperature. It is ∼1.6 in the low temperature range, decreases rapidly above ∼80 K, and takes a value of ∼1.15 at the temperature of 120 K (inset in figure 11). We have tried different t values between 1 and 2 and found that only small t can reproduce the rapid decrease of ρ near $m = f_c$ when the temperature is between 90 and 120 K. Calculations are not performed for temperatures above 120 K because of the relatively small resistivity change under the applied field. According to percolation theory, the parameter t varies
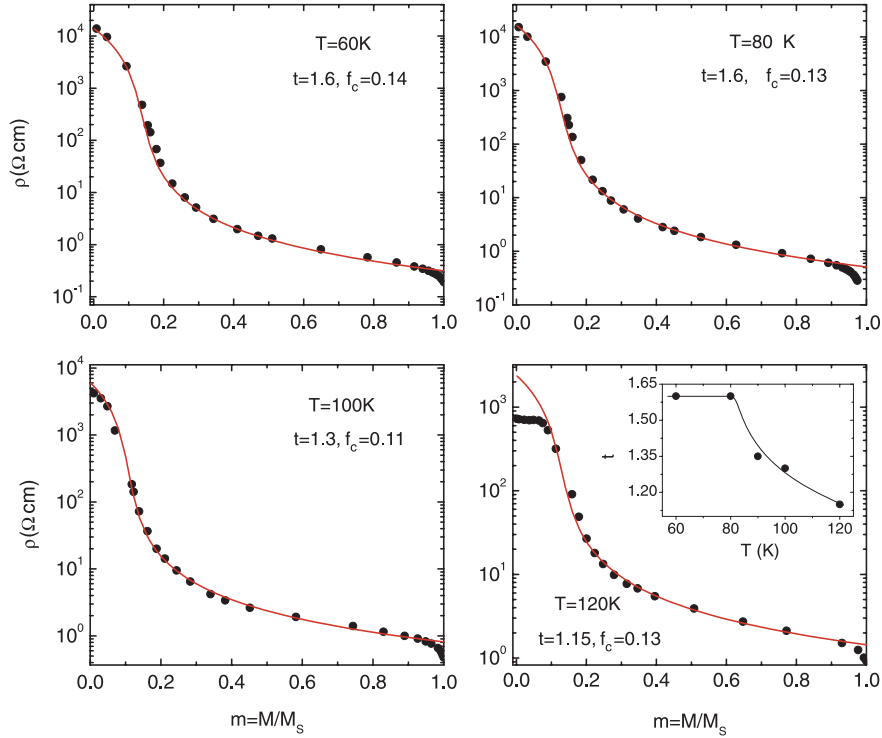
Figure 11. Observed (symbols) and calculated (solid lines) ρ–m relations of LNCMO for selected temperatures between 60 and 120 K. The inset plot displays the variation of the critical exponent with temperature. The solid line in the inset plot is a guide for the eyes.

between 1.6 and 2 for a three-dimensional system while it is between 1 and 1.4 for a two-dimensional one [33, 34]. The tendency for t to unity may indicate the decrease of the effective dimensionality of the system as temperature increases. In the temperature range through which T_C sweeps under the driving of the applied field (90–150 K), the magnetic field could affect both the shape and spatial distribution of the FM domains, which will amend the percolation process and thus the ρ–m relation. The critical exponent adopted in the present analysis is considerably smaller than that used by Kim *et al* for La$_{5/8-x}$Pr$_x$Ca$_{3/8}$MnO$_3$ [7]. The phase separation has been tuned by Pr content in La$_{5/8-x}$Pr$_x$Ca$_{3/8}$MnO$_3$ while by the applied magnetic field in LNCMO.

Considerable deviations of experiment data from calculated results emerge and develop as m approaches saturation. This behavior reflects the intrinsic property of the FM phase considering the fact that only the FM phase survives in this case. Effects produced by the growth of FM domains and the spin alignment in FM domains could be different. The latter is much more effective in affecting conduction. As shown in figure 8, the resistivity decreases from ~1 to ~0.2 Ω cm as m increases from ~0.9 to ~1 (marked by two arrows), as a result of the depression of thermal fluctuation of the FM domains by the magnetic field. In contrast, generally a reduction in resistivity of one order of magnitude requires a variation of m from ~0.3 to ~0.9 when it is produced by the growth of FM fraction. The isothermal M–$\mu_0 H$ data, for example, at 50 K, show that the magnetization of the FM phase grows from ~90.6 to ~94.7 emu g^{-1} as the magnetic field increases from 0 to 5 T. Δm is only ~0.04. It is therefore difficult to determine an exact ρ–m dependence for the FM phase simply based on the data
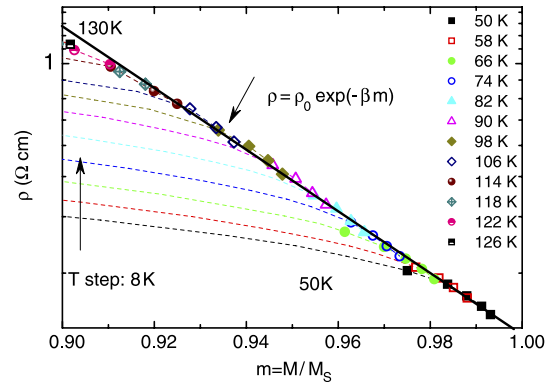

Figure 12. Resistivity as a function of normalized magnetization for the FM phase of LNCMO. Symbols and dashed lines denote the ρ–m curves of the FM state and the FM + PM/AFM state, respectively. Data collected at different temperatures are marked by different symbols. Solid lines are guides for the eyes.

at a fixed temperature due to the small Δm. It is fortunate that the magnetization of the FM phase varies significantly with the increase of temperature. M is ~94.7 emu g^{-1} at $T = 50$ K and ~86.8 emu g^{-1} for $T = 120$ K under a fixed field of 5 T. This provides a Δm span wide enough for an accurate determination of the ρ–m relation. By analyzing the ρ–m curves of the FM phase under various temperatures (marked by the solid symbols in figure 12), which collapse into the same line, we obtain a relation $\rho = \rho_0 \exp(-\beta m)$ with $\beta \approx 22.2$. It is an equation similar to that of Hundley *et al* in the form [16]. However, the coefficient β of LNCMO is significantly larger (~22.2 versus

~4.4). The different β values may reflect the intrinsic difference of the resistive responses to the change of magnetic order near T_C and well below T_C. In fact, the distinctive ρ–m dependence of the FM phase has been observed before in special manganese oxides. A typical example is the oxygen-deficient $La_{0.67}Ba_{0.33}MnO_{3-\delta}$ in which a continuous resistivity decrease occurs, with the increase of magnetic field, while magnetization is nearly saturated [35].

3.5. Discussion

As revealed by the magnetic data, even at low temperatures a field of 2 T can drive LNCMO from an AFM state into an FM state. This implies that the difference in internal energy of these two states is smaller than $\Delta U = HM \approx 180$ J kg^{-1}, where M has been set to 90 emu g^{-1}. As shown in figure 2, the compound is totally FM at low temperatures above 2 T, and reenters into an AFM state slightly above T_C if $\mu_0 H < 3$ T. Considering the fact that the two phases will have the same free energy at T_C, a simple estimation gives the entropy change under a field of, for example, 2.5 T, $\Delta S = (HM - \Delta U)/T_C \approx 0.17$ J kg^{-1}, where $T_C \approx 120$ K and $M \approx 80$ emu g^{-1} (a value near T_C) have been adopted. This analysis indicates that the entropy change accompanying the AFM–FM transition could be quite small, which explains the invisibility of the thermal anomaly near T_C when the magnetic field is low.

Similar phenomena were also observed in other phase-separated manganites. It has been reported that there are no visible thermal anomalies in heat capacity corresponding to the magnetic transition at ~70 K of $La_{5/8-y}Pr_yCa_{3/8}MnO_3$ ($y = 0.35$), even for a carefully controlled experiment [8]. Kiryukhin and collaborators ascribed this phenomenon to the percolation character of this phase transition. Similar behaviors are also observed for the field-induced FM transition at ~100 K in single-crystal $Pr_{0.63}Ca_{0.37}MnO_3$, for which an AFM transition occurs at ~170 K [36]. Therefore, it could be a general conclusion that the thermal effects will be greatly depressed if the FM transition is induced by an external field in an AFM matrix. However, when the long range AFM order is partially destroyed by, for example, element doping, the corresponding entropy change may reappear. This is the case occurring in $Pr_{0.5}Ca_{0.5}Mn_{0.95}Ga_{0.05}O_3$, for which a considerable anomaly at the FM transition can be detected by heat capacity [37].

The distinctive behavior of ΔS may have a strong impact on the variation of T_C under an applied field. It could be instructive to compare the T_C–$\mu_0 H$ and ΔS–$\mu_0 H$ relations. A general tendency to a gradual reduction in $\Delta T_C/\Delta H$ with the increase of ΔS can be identified. This coincidence may not be an accident. The Clausius–Clapeyron equation predicts $\Delta T_C = \Delta H \Delta M/\Delta S$, that is, ΔT_C decreases as ΔS grows, where ΔM is the magnetization change accompanying the first-order magnetic transition and ΔT_C is the increment of Curie temperature under an external field. Based on this formula, the largest $\Delta T_C/\Delta H$ may appear near 2 T, where ΔM is maximum while ΔS is minimum (figure 6). However, due to the pinning of T_C to ~90 K in the low field range, which influences the subsequent T_C–H relation,

the most rapid change of T_C appears near 3 T. In the case of $\mu_0 H > 6$ T, a simple estimate shows that $\Delta T_C/\Delta H = \Delta M/\Delta S \approx 7.5$ K T^{-1}, where ΔS takes the saturation value (~4 J kg^{-1} K^{-1}) and $\Delta M \approx 30$ emu g^{-1}. This result is consistent with the value directly extracted from figure 3, $\Delta T_C/\Delta H \approx 6.8$ K T^{-1}, under the fields above 6 T. Considering the fact that the entropy change accompanying the FM–AFM transition is usually smaller than that produced by an FM–PM transition, we can safely say that it is easier for the magnetic field to induce the FM phase in the AFM background than in the PM one.

Based on the previous analyses, the transport behavior of the manganites can be described by a general equation (equation (2)). It would be instructive to note the similarity of equation (2) to the standard formula [38]

$$\rho = A_0 T \exp\left(\frac{\varepsilon' - \eta}{T}\right), \quad (4)$$

for the polaronic conduction, where η is the transfer integral. Equation (4) reveals the importance of bandwidth for the electronic transport in manganites. In general, η is nearly independent of temperature and is not explicitly involved in the formula. For the manganites, however, thermal spin fluctuation will certainly affect bandwidth, and thus charge transferring. This actually implies the temperature dependence of η. According to the double exchange theory, the conduction in manganites proceeds via the migration of e_g electrons between Mn^{3+} and Mn^{4+} ions with a transfer integral of $\eta' = \eta_0 \cos(\psi/2)$, where ψ is the angle between two adjacent spins of Mn ions. Approximating η by η', a direct calculation based on the mean field approximation shows

$$\eta = \eta_0 \sqrt{\frac{1 + \langle \cos \psi \rangle}{2}} \approx \eta_0 \left(\frac{1 + m^2/2}{\sqrt{2}}\right), \quad (5)$$

where $\langle A \rangle$ denotes the statistical average of A and the equality $\langle \cos \psi \rangle = m^2$ has been used in the derivation [39]. The expansion in equation (5) demands that m is small, which can be readily satisfied in the PM state. Inserting equation (5) into equation (4), we obtain

$$\rho = A_0 T \exp\left(\frac{\varepsilon' - \eta_0/\sqrt{2} - \eta_0 m^2/2\sqrt{2}}{T}\right). \quad (6)$$

Equation (6) is the same in form as equation (2) after setting $\alpha = \eta_0/2\sqrt{2}$ and $\varepsilon = \varepsilon' - \eta_0/\sqrt{2}$. It has been experimentally proved that η_0 varies between 0.1 and 0.2 eV for the hole-doped manganites [40], which implies $\alpha \approx 400$–810 K, in reasonable agreement with the observed $\alpha \approx 800$ K.

The above results suggest that the activation energy derived from the ρ–T relation includes the effect of magnetization, and the increase of m enhances the probability of polaron transfer. This result explains the usually detected reduction of activation energy in the presence of an external field. It also predicts a possible deviation of the $\ln(\rho/T)$–$1/T$ relation from linearity because of the temperature dependence of m.

In addition to the rapid variation of resistivity with percolation, the great difference from the simple relation

obtained for La$_{0.7}$Ca$_{0.3}$MnO$_3$ [16] is the dispersion of ρ–m curves with temperature above the percolation threshold. As seen in figure 8(a), the change in resistivity can be as large as one order of magnitude, from ∼0.1 to ∼1 Ω cm, as temperature increases from 50 to 120 K when m is fixed. It is one of the typical behaviors resulting from phase separation. In the picture of phase separation, conduction of the compound is jointly determined by coexisting phases. Even when the proportions of the metallic and insulating phases are fixed, the overall conductivity of the mixed phase will change with temperature. When the temperature is low, the increase of resistivity with temperature could mainly originate from the increase of the resistivity of the FM phase, as a consequence of enhanced thermal spin fluctuation. In contrast, even when m is relatively high, a tendency of resistivity decrease can appear at high temperatures, where the conductivity of PM phase increases exponentially with temperature and becomes comparable with that of the FM phase. Therefore, phase separation yields a much more complex ρ–m dependence.

4. Summary

In summary, the magnetic, resistive and thermal properties of La$_{0.27}$Nd$_{0.4}$Ca$_{0.33}$MnO$_3$ have been experimentally studied. The compound is found to exhibit a complex behavior with the variation of temperature and magnetic field. Without an external field, it stabilizes in the charge/orbital ordered AFM state. In the presence of a field between 0.5 and 2 T, the compound undergoes first a charge/orbital ordering transition at $T_{CO} \sim 175$ K then an AFM transition at $T_N \sim 156$ K and, finally, an FM transition around $T_C \sim 110$ K, with a significant tendency for T_C to increase with applied field. The FM and AFM phases coexist in a wide temperature range below the Curie temperature. Based on these data, a magnetic phase diagram that shows the evolution of the FM, AFM and PM phases with magnetic field and temperature is established.

The magnetic entropy change accompanying the field-induced FM transition is negligibly small when T_C is well below T_N, increases rapidly as T_C approaches T_N and saturates at a value of ∼4 J kg^{-1} K^{-1} for $T_C > T_N$. These could be general features of the thermal effects of this kind of phase transition, because of the comparable stability of FM and AFM phases.

Quantitative descriptions of the magnetic–resistive correlation are studied for the PM phase, the FM phase and the mixed FM and PM phases, respectively. For the PM phase, a polaronic transport behavior $\rho = A_0 T \exp[(\varepsilon - \alpha m^2)/T]$ ($\alpha \approx 800$ K) with a magnetization-tuned activation energy is observed (Boltzmann's constant k_B has been set to unity), where m is the normalized magnetization. It could be a general feature in manganites, appearing also in other compounds with different characteristics such as La$_{0.67}$Ca$_{0.33}$MnO$_3$ films and La$_{0.474}$Bi$_{0.193}$Ca$_{0.33}$Mn$_{0.994}$Cr$_{0.006}$O$_3$ and Eu$_{0.55}$Sr$_{0.45}$MnO$_3$ ceramics. Based on the double exchange theory, the physical background of this relation is discussed. The effective medium theory provides a satisfactory description for the ρ–m relation of the FM and AFM mixed state with, however, a reduction of the effective dimensionality of the system from three

to two when the temperature enters into the regime through which T_C sweeps under the driving of a magnetic field. In the FM state, the resistivity is quite sensitive to the change of spin alignment and exhibits an exponential decrease with magnetization $\rho = \rho_0 \exp(-\beta m)$ at a rate ($\beta \approx 22.7$) much higher than that predicted by Hundley *et al* ($\beta \approx 4.4$) [16], which could be a universal relation since it is also observed in rather different manganites. The field-induced phase separation is believed to be responsible for the distinctive properties of La$_{0.27}$Nd$_{0.4}$Ca$_{0.33}$MnO$_3$.

Acknowledgments

References

[1] Jin S, Tiefel T H, McCormack M, Fastnacht R A, Ramesh R and Chen L H 1994 *Science* **264** 413
Hwang H Y, Cheong S W, Ong N P and Batlogg B 1996 *Phys. Rev. Lett.* **77** 2041
[2] For a review, see Rao C N R and Raveau B (ed) 1998 *Colossal Magnetoresistance, Charge ordering, and Related Properties of Manganese Oxides* (Singapore: World Scientific)
Tokura Y (ed) 1999 *Colossal Magnetoresistance Oxides* (London: Gordon and Breach)
Salamon M B and Jaime M 2001 *Rev. Mod. Phys.* **73** 583
[3] Asamitsu A, Tomioka Y, Kuwahara H and Tokura Y 1997 *Nature* **388** 50
[4] Miyano K, Tanaka T, Tomioka Y and Tokura Y 1997 *Phys. Rev. Lett.* **78** 4257
[5] Itoh M, Nishi K, Yu J D and Inaguma Y 1997 *Phys. Rev.* B **55** 14408
[6] Uehara M, Mori S, Chen C H and Cheong S W 1999 *Nature* **399** 560
[7] Kim K H, Uehara M, Hess C, Sharma P A and Cheong S-W 2000 *Phys. Rev. Lett.* **84** 2961
[8] Kiryukhin V, Kim B G, Podzorov V, Cheong S-W, Koo T Y, Hill J P, Moon I and Jeong Y H 2000 *Phys. Rev.* B **63** 024420
[9] Rao G H, Sun J R, Liang J K and Zhou W Y 1997 *Phys. Rev.* B **55** 3742
[10] Fäth M, Freisem S, Menovsky A A, Tomioka Y, Aarts J and Mydosh J A 1999 *Science* **285** 1540
[11] Becker T, Streng C, Luo Y, Moshnyaga V, Damaschke B, Shannon N and Samwer K 2002 *Phys. Rev. Lett.* **89** 373203
[12] Wu T and Mitchell J F 2006 *Phys. Rev.* B **74** 214423
[13] Asamitsu A, Tomioka Y, Kuwahara H and Tokura Y 1997 *Nature* **388** 50
[14] Babushkina N A, Belova L M, Khomskii D I, Kugel I, Gorbenko O Yu and Kaul A R 1999 *Phys. Rev.* B **59** 6994
[15] Tokunaga M, Tokunaga Y and Tamegai T 2004 *Phys. Rev. Lett.* **93** 037203
[16] Hundley M F, Hawley M, Heffner R H, Jia Q X, Neumeier J J, Tesmer J, Thompson J D and Wu X D 1995 *Appl. Phys. Lett.* **67** 860
[17] Urushibara A, Moritomo Y, Arima T, Asamitsu A, Kido G and Tokura Y 1995 *Phys. Rev.* B **51** 14103
[18] Chen B, Uher C, Morelli A T, Mantese J V, Mance A M and Micheli A L 1996 *Phys. Rev.* B **53** 5094

[19] Sundaresan A, Maignan A and Raveau B 1997 *Phys. Rev.* B **55** 5596

[20] Wang J Z, Sun J R, Liu G J, Xie Y W, Wang D J, Zhao T Y, Shen B G and Li X G 2007 *Phys. Rev.* B **76** 104428

[21] Tomioka Y, Hiraka H, Endoh Y and Tokura Y 2006 *Phys. Rev.* B **74** 104420

[22] Tomioka Y, Asamitsu A, Kuwahara H and Tokura Y 1997 *J. Phys. Soc. Japan* **66** 302

[23] Sun J R, Gao J, Fei Y, Li R W and Shen B G 2003 *Phys. Rev.* B **67** 144414

[24] Xiong C M, Sun J R, Chen Y F, Shen B G, Du J and Li Y X 2005 *IEEE Trans. Magn.* **41** 122

[25] Sun J R, Yeung C F, Zhao K, Zhou L Z, Leung C H, Wong H K and Shen B G 2000 *Appl. Phys. Lett.* **76** 1164

[26] Abramovich A I, Gorbenko O Yu, Kaul A R, Koroleva L I and Michurin A V 2004 *J. Exp. Theor. Phys.* **99** 820
Abramovich A I, Koroleva L I and Michurin A V 2002 *J. Exp. Theor. Phys.* **95** 917

[27] Nagaev E L 2001 *Phys. Rep.* **346** 381
Dagotto E, Hotta T and Moreo A 2001 *Phys. Rep.* **344** 1

[28] Sacanell J, Levy P, Leyva A G, Parisi F and Ghivelder L 2007 *J. Phys.: Condens. Matter* **19** 186226

[29] Millange F, Brion S and Chouteau G 2000 *Phys. Rev.* B **62** 5619

[30] Gordon J E, Fisher R A, Jia Y X, Phillips N E, Reklis S F, Wright D A and Zettl A 1999 *Phys. Rev.* B **59** 127

[31] Liu G L, Zhou J S and Goodenough J B 2001 *Phys. Rev.* B **64** 144414
Liu G L, Zhou J S and Goodenough J B 2004 *Phys. Rev.* B **70** 224421

[32] Liu G J, Sun J R, Xie Y W, Wang D J, Xiong C M, Zhang H W, Zhao T Y and Shen B G 2005 *Appl. Phys. Lett.* **87** 182502
Kiryukhin V, Kim B G, Podzorov V, Cheong S-W, Koo T Y, Hill J P, Moon I and Jeong Y H 2000 *Phys. Rev.* B **63** 024420

[33] Deutscher G, Zallen R and Adler J (ed) 1983 *Percolation Structures and Processes* (Bristol: Hilger) p 220

[34] Bernasconi J 1978 *Phys. Rev.* B **18** 2185

[35] Ju H L, Gopalakrishnan J, Peng J L, Li Q, Xiong G C, Venkatesan T and Greene R L 1995 *Phys. Rev.* B **51** 6143

[36] Raychaudhuri A K, Guha A, Das I, Rawat R and Rao C N R 2001 *Phys. Rev.* B **64** 165111

[37] Hardy V, Maignan A, Hébert S and Martin C 2003 *Phys. Rev.* B **67** 024401

[38] Salamon M B and Jaime M 2001 *Rev. Mod. Phys.* **73** 583

[39] Viret M, Ranno L and Coey J M D 1997 *Phys. Rev.* B **55** 8067

[40] Millis A J, Littlewood P B and Shraiman B I 1995 *Phys. Rev. Lett.* **74** 5144